Journal of Engineering Physics and Thermophysics, Vol. 75, No. 4, 2002

MODELING OF THE IMPACT OF A BUBBLE-LIQUID DROPLET

V. S. Surov

UDC 532.525.6

Since a bubble liquid has a low wave resistance as compared to the resistance of a pure liquid and a strongly nonlinear compression-test diagram, the quantitative characteristics of interaction on impact will differ from the analogous ones for the case of the liquid without gas occlusions. The distinctive features of the phenomenon of impact of the droplets of a bubble liquid on rigid or deformable obstacles have been described; the calculations have been performed within the framework of the generalized-equilibrium model of the bubble liquid.

Apart from the fact that the phenomenon of collision of droplets of a liquid with the surface of a solid body is of scientific interest, it is also of practical importance in many fields of technology. Turbine blading and elements of aircraft-spacecraft are subject to high-velocity shock loading in flights in the rainy zone. In recent times, interest has been aroused in application of high-velocity liquid jets in the mining industry in sinking oil and gas wells and in cutting mechanically different materials and cleaning their surfaces. The impact of a droplet is frequently preceded by the stage of its passage through a layer of a strongly compressed gas; the surface layer of the droplet is saturated with the gas [1]. It is well known that the properties of a gas-liquid mixture are significantly different from the properties of a liquid without gas occlusions [2]; therefore, it is of interest to study the influence of the concentration of the gas in a liquid on the process of interaction of a droplet with an obstacle. The impact of a droplet has been investigated in the literature [3–7]; however, in all works it has been assumed that the liquid contains no gas occlusions. In the work presented, in describing the phenomenon of impact of a droplet, we employ a generalized-equilibrium model in which small-scale bubble pulsations are disregarded. Within the framework of this model, flows of a dispersive medium can be investigated in a wide range of variation of the concentration of the gas in the mixture: from foamy liquids to bubble ones [8].

1. One-Dimensional Calculations. Let us consider the flow produced by the impact of the homogeneous semiinfinite mass of a bubble liquid, having the volume fraction of the gas α_0 and moving with the velocity u_0, upon a rigid flat obstacle. After the collision, a shock wave (SW) moving with velocity $-D$ in a coordinate system which is tied to the obstacle is formed. Behind its front, the bubble liquid compressed to the pressure p' (at an initial p_0) is at rest. In passage through the SW front, the Rankine–Hugoniot relations

$$(\rho' - \rho_0)(-D) = -\rho_0 u_0\,, \quad \rho_0 u_0 D = p' - p_0 - \rho_0 u_0^2\,, \tag{1}$$

written for the entire mixture are true; this, in particular, yields the formula to calculate the pressure of a hydraulic shock $p' = p_0 + \rho_0 u_0 (u_0 + D)$. The primed parameters correspond to the quantities behind the shock front. The last expression will be written in dimensionless form

$$\tilde{p}' = 1 + \tilde{p}_0 + \tilde{D}\,, \tag{2}$$

where $\tilde{p}' = p'/(\rho_0 u_0^2)$, $\tilde{p}_0 = p_0/(\rho_0 u_0^2)$, and $\tilde{D} = D/u_0$. In the case of impact, upon the obstacle, of a binary mixture with one incompressible component whose shock adiabat has the form [8]

$$\rho_0/\rho' = \alpha_0 (\chi p' + p_0)/(\chi p_0 + p') + 1 - \alpha_0\,, \quad \chi = (\gamma - 1)/(\gamma + 1)\,, \tag{3}$$

Chelyabinsk State University, Chelyabinsk, Russia; email: svs@csu.ru. Translated from Inzhenerno-Fizicheskii Zhurnal, Vol. 75, No. 4, pp. 135–140, July–August, 2002. Original article submitted August 28, 2001; revision submitted October 15, 2001.

1062-0125/02/7504-0934$27.00

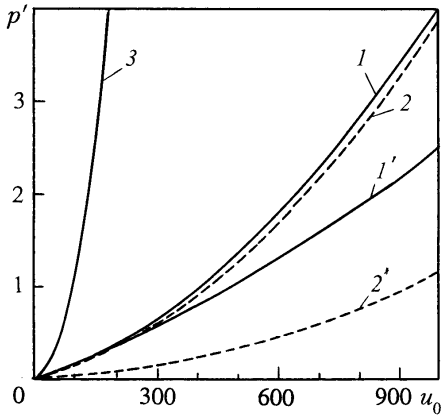

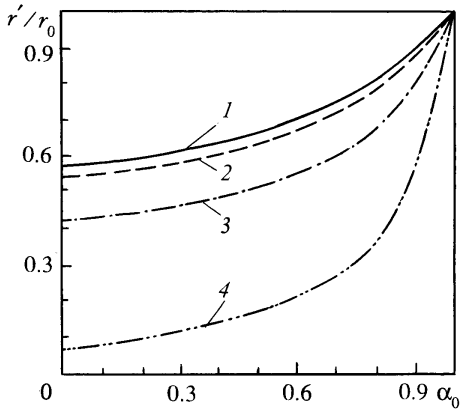

Fig. 1. Dependences of p' on u_0 at $\alpha = 0$ (1 and 1′) and 0.01 (2, 2′, and 3). Curves 1′ and 2′, within the framework of acoustic approximation; curve 3, disregarding the compressibility of the liquid fraction. p', GPa.

Fig. 2. Dependences $r'/r_0(\alpha_0)$ for a water-gas mixture with N_2, H_2, and He bubbles and according to the isothermal model (1–4 respectively) for $u_0 = 200$ m/sec.

where γ is the adiabatic exponent of the gas component of the mixture, we have the following relation to calculate the velocity of movement of the SW front:

$$\tilde{D} = \left(2\alpha_0 (\chi - 1) + 1 + \sqrt{1 + 4\alpha_0 \tilde{p}_0 (1 - \chi^2)}\right) / (2\alpha_0 (1 - \chi)), \tag{4}$$

which follows from (1)–(3). The equation to calculate the dimensionless SW velocity $\tilde{D}$ obtained with allowance for the compressibility of the liquid fraction has the form

$$\tilde{D}/(1 + \tilde{D}) = \alpha_0 \chi (1 + \tilde{D}) + \frac{(\chi + 1)\tilde{p}_0}{1 + \tilde{D} + (\chi + 1)\tilde{p}_0} + (1 - \alpha_0) \frac{\chi_1 (1 + \tilde{D}) + (\chi_1 + 1)(\tilde{p}_0 + \tilde{p}_{\bullet 1})}{1 + \tilde{D} + (\chi_1 + 1)(\tilde{p}_0 + \tilde{p}_{\bullet 1})}. \tag{5}$$

Here $\chi_1 = (\gamma_1 - 1)/(\gamma_1 + 1)$, $\tilde{p}_{\bullet 1} = p_{\bullet 1}/\rho_0 u_0^2$), and $p_{\bullet 1} = \rho_{\bullet 1} c_{\bullet 1}^2/\gamma_1$; $\rho_{\bullet 1}$, $c_{\bullet 1}$, and γ_1 are the constants of the liquid component of the mixture for the binomial equation of state [8]

$$\varepsilon_i = (p - c_{\bullet i}^2 (\rho_i^0 - \rho_{\bullet i}))/((\gamma_i - 1)\rho_i^0), \tag{6}$$

employed here and in Sec. 2 to describe the properties of the constituent components of the mixture and of the obstacle material. For example, the corresponding constants of Eq. (6) have values of $\rho_{\bullet 1} = 1000$ kg/m^3, $c_{\bullet 1} = 1515$ m/sec, and $\gamma_1 = 5.59$ for water and $\rho_{\bullet 2} = 8930$ kg/m^3, $c_{\bullet 2} = 4200$ m/sec, and $\gamma_2 = 3.183$ for copper.

Figure 1 shows the dependences of the pressure of a hydraulic shock on the rate of interaction of a liquid mass with a solid obstacle which have been obtained in the absence of gas occlusions in the liquid and in the presence of 1% of air in it. Additional calculations were carried out within the framework of acoustic approximation; the velocity of movement of the SW front was assumed to be equal to the velocity of sound in the bubble liquid, i.e., $D = c_0$. It is well known that for a liquid without gas occlusions the use of the acoustic approximation makes it possible to obtain results coincident, in practice, with the "exact" ones for impact velocities of up to several hundred meters per second [4], which, in particular, is confirmed by the data in Fig. 1. Furthermore, the figure shows that the presence of a low amount of air in the liquid eliminates the possibility of using the acoustic approximation even when the impact velocity is low, which is related to the strong linear dependence of the properties of the bubble liquid on the concentration of gas in the mixture: small variations of the concentration of the gas correspond to significant changes in other quantities. We also note that for the class of (shock-type) problems considered it is necessary to take into account the compressibility of the liquid component, which is of particular importance for bubble liquids since the discrepancies, for example, in pressure obtained for them with allowance for the compressibility of the carrier fraction

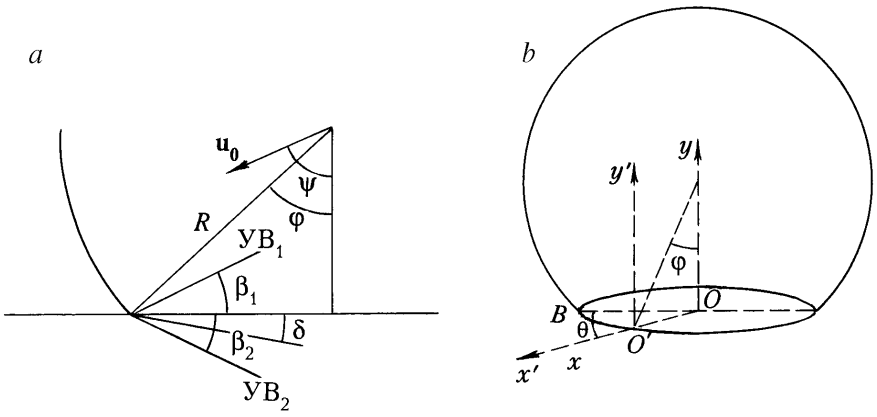

Fig. 3. Flow diagram in the case of impact of a spherical droplet of a bubble liquid against a compressible obstacle.

and without allowance for it increase without bound with increase in the impact velocity as the volume fractions of the gas in the mixture decreases (Fig. 1). When the air in the bubbles is replaced by other gases (consideration was given to nitrogen, hydrogen, and helium) such parameters as the velocity of movement of the SW and the pressure behind its front depend weakly on the type of gas. The volume fraction of the gas in the mixture behind the shock front is a more sensitive parameter. If we assume that the bubbles in the liquid in an undisturbed state had a spherical shape with equal radii r_0, the change in the latter behind the SW front can be calculated from the relation

$$r'/r_0 = (\alpha'/\alpha_0)^{1/3}.$$

Figure 2 shows the dependences $r'/r_0(\alpha_0)$ for different gases in bubbles; it is seen that in the case of impact the bubbles, calculated according to the isothermal model of a dispersive medium [8] and whose radius decreases by approximately an order of magnitude for the initial concentration α_0 to 0.3, are compressed to the greatest extent. When the isothermal model with an incompressible carrier liquid is employed the bubbles behind the shock front disappear totally.

2. Initial Stage of Impact of a Spherical Droplet of a Bubble Liquid on a Deformable Obstacle. The normal impact of a spherical droplet of water (without gas occlusions) on a rigid obstacle has been considered in [9] for the first time. The glancing impact of a spherical droplet of water, without gas occlusions as well, on a deformable obstacle has been investigated in [10]. A distinctive feature of the impact of droplets with a convex forepart against an obstacle is that at the initial stage of impact where the velocity of movement of the contact line is higher than the velocity of propagation of the SW in a bubble liquid, the pressure maximum moves to the periphery of the contact spot and is not located at the center, where the pressure coincides with the pressure of a one-dimensional hydraulic impact calculated from formula (2). In the present section, we have studied the influence of the gas content on the flow parameters of the initial stage of the glancing impact of a spherical droplet for the regime of an SW attached to the perimeter of the contact spot. Just as in [10], account is taken of the compressibility of the obstacle material, which is necessary if the impact velocity is several hundred meters per second.

Let the spherical droplet touch the obstacle at point O at the instant of time $t = 0$. We tie the Cartesian coordinate system to point O and arrange the coordinate axis Ox along the obstacle surface. In this coordinate system, the velocity vector of the droplet $\mathbf{u}_0$ is directed to the Oy axis at an angle ψ. The impact of a droplet with a convex forepart can be represented as the collision of a droplet with an obstacle for an angle of inclination of the free surface of the droplet to the obstacle $\varphi = \varphi(t)$ varying with time. For example, in the case of impact of a spherically shaped droplet of radius R, the indicated dependence follows from geometric considerations (Fig. 3a) and has the form

$$\varphi = \arccos\,(1 - |\mathbf{u}_0|\, t \cos\psi/R)\,. \tag{7}$$

We introduce a moving coordinate system $x'O'y'$ by placing point O' on the boundary of the contact spot (Fig. 3b). In this moving coordinate system, the flows of the bubble liquid and of the obstacle material are equal to $\mathbf{u}_0 + \mathbf{u}_c$ and $\mathbf{u}_c$ respectively ($\mathbf{u}_c$ is the velocity of the contact boundary in the coordinate system xOy; $|\mathbf{u}_c| = |\mathbf{u}_0|$ (cos ψ tan

$\varphi + \cos\,\theta\,\sin\,\psi)$). By decomposing these vectors into the normal and tangential components to the attached SW_1 and SW_2 (Fig. 3a) which propagate over the droplet and the obstacle material, we obtain

$$u_{1n} = |\mathbf{u}_0|\,[(\cos\psi/\tan\varphi + \cos\theta\sin\psi)\sin\beta_1 + \cos\psi\cos\beta_1]\,,$$
$$u_{1t} = |\mathbf{u}_0|\,[(\cos\psi/\tan\varphi + \cos\theta\sin\psi)\cos\beta_1 - \cos\psi\sin\beta_1]\,, \tag{8}$$
$$u_{2n} = |\mathbf{u}_0|\,(\cos\psi/\tan\varphi + \cos\theta\sin\psi)\sin\beta_2\,,$$
$$u_{2t} = |\mathbf{u}_0|\,(\cos\psi/\tan\varphi + \cos\theta\sin\psi)\cos\beta_2\,,$$

where the subscripts *i*n and *i*t denote the normal and tangential components of the velocity vectors to the attached SW_i ($i = 1, 2$) and θ is the angle between the radius to a point on the perimeter of contact (OO') and the projection of the velocity vector $\mathbf{u}_0$ onto the plane of the contact spot (OB).

For the SW_1 and SW_2 attached to the perimeter of the contact spot the Rankine–Hugoniot relations take the form

$$\rho_{10}u_{1n} = \rho_1'u_{1n}',\quad p_1' = p_0 + \rho_{10}u_{1n}(u_{1n} - u_{1n}')\,,$$
$$\rho_{20}u_{2n} = \rho_2'u_{2n}',\quad p_2' = p_0 + \rho_{20}u_{2n}(u_{2n} - u_{2n}')\,. \tag{9}$$

Taking into account that the pressure is continuous in passage through the contact discontinuity, we have

$$p_1' = p_2' = p'\,. \tag{10}$$

Since the velocity vectors $\mathbf{u}_1'$ and $\mathbf{u}_2'$ are parallel to the plane of contact discontinuity, the relations

$$u_{1n}' = u_{1t}\tan(\beta_1 + \delta)\,,\quad u_{2n}' = u_{2t}\tan(\beta_2 + \delta)\,, \tag{11}$$

are true, where account is also taken of the equality of the tangential components of the velocities ahead of the fronts of the attached SW_1 and SW_2 and behind them, i.e., $u_{1t}' = u_{1t}$ and $u_{2t}' = u_{2t}$. The shock adiabats of the gas-liquid mixture with a compressible liquid component and of the obstacle material with account for (8)–(11) take the form

$$\frac{\tan(\beta_1 + \delta)\,[(\cos\psi/\tan\varphi + \cos\theta\sin\psi)\cos\beta_1 - \cos\psi\sin\beta_1]}{(\cos\psi/\tan\varphi + \cos\theta\sin\psi)\sin\beta_1 + \cos\psi\cos\beta_1} = \alpha_0\,\frac{\chi\,\rho_{10}u_{1n}(u_{1n} - u_{1t}\tan(\beta_1 + \delta)) + p_0(\chi + 1)}{\rho_{10}u_{1n}(u_{1n} - u_{1t}\tan(\beta_1 + \delta)) + p_0(\chi + 1)} +$$
$$+ (1 - \alpha_0)\,\frac{\chi_1\,\rho_{10}u_{1n}(u_{1n} - u_{1t}\tan(\beta_1 + \delta)) + (p_0 + p_{\bullet 1})(\chi_1 + 1)}{\rho_{10}u_{1n}(u_{1n} - u_{1t}\tan(\beta_1 + \delta)) + (p_0 + p_{\bullet 1})(\chi_1 + 1)}\,, \tag{12}$$

$$\tan(\beta_2 - \delta)/\tan\beta_2 = \frac{\chi_2\,\rho_{20}u_{2n}(u_{2n} - u_{2t}\tan(\beta_2 - \delta)) + (p_0 + p_{\bullet 2})(\chi_2 + 1)}{\rho_{20}u_{2n}(u_{2n} - u_{2t}\tan(\beta_2 - \delta)) + (p_0 + p_{\bullet 2})(\chi_2 + 1)}\,, \tag{13}$$

where $\chi_2 = (\gamma_2 - 1)/(\gamma_2 + 1)$ and $p_{\bullet 2} = \rho_{\bullet 2}c_{\bullet 2}^2/\gamma_2$; $\rho_{\bullet 2}$, $c_{\bullet 2}$, and γ_2 are the constants of the binomial equation of state (6) for the obstacle material. Expression (10) yields another relation which, with account for (9) and (11), takes the form

$$\rho_{20}u_{2n}(u_{2n} - u_{2t}\tan(\beta_2 - \delta)) = \rho_{10}u_{1n}(u_{1n} - u_{1t}\tan(\beta_1 + \delta))\,. \tag{14}$$

The system of three nonlinear relations (12)–(14) enables us to calculate the unknown angles β_1, β_2, and δ and, using them, also the remaining parameters of the problem.

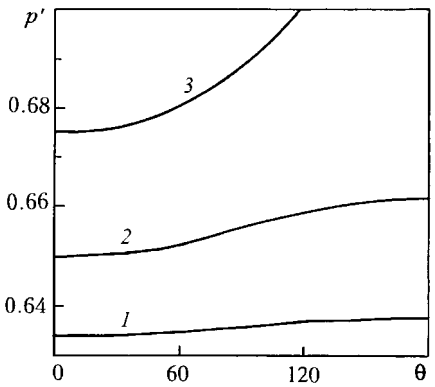

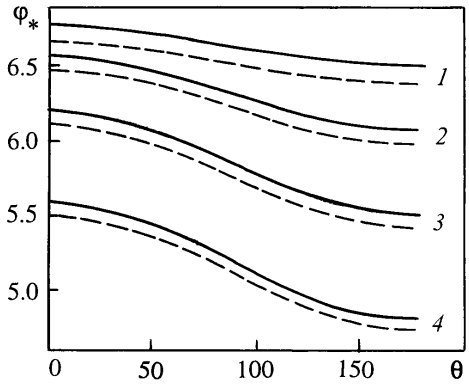

Fig. 4. Dependences $p'(\theta)$ for $\varphi = 3$, 4, and 5^o (1–3 respectively) on impact of a droplet ($\alpha_0 = 0.1$, $u_0 = 500$ m/sec, and $\psi = 40^o$) against a copper obstacle. p', MPa.

Fig. 5. Dependences $\varphi_*(\theta)$ on impact of a droplet ($u_0 = 500$ m/sec) against a copper obstacle for $\psi = 10$, 20, 30, and 40^o (1–4 respectively); solid curves, at $\alpha = 0.1$; dashed curves, $\alpha_0 = 0$.

Figure 4 gives the dependences of the pressure p' on the angle θ obtained in calculations of the impact of a water droplet with an initial gas content of $\alpha_0 = 0.1$ against a copper obstacle. The angle of inclination of the velocity vector is $\psi = 40^o$ and the impact velocity is $u_0 = 500$ m/sec. From the figure it is clear that the distribution of the parameters over the perimeter of the contact spot is nonuniform; the nonuniformity increases with increase in the angle φ and in the angle ψ. This, in particular, is clear from Fig. 5, which shows the dependences of the critical angle φ_* on the angle θ calculated for different angles of inclination of the velocity vector of the droplet ψ in the case of its impact against a copper obstacle. The critical angle φ_* is the largest angle of contact φ for which the flow regime with shock waves attached to the contact point is still possible or, what is the same, the solution of the system of equations (12)–(14) still exists. For an angle of contact φ larger than the critical φ_* the velocity of disturbances propagating over the obstacle is higher than the velocity of movement of the contact-spot boundary: in this case we observe the "swelling" of the obstacle surface behind the contact point. As the concentration of gas in the droplet increases the pressure p' decreases, which is related to the decrease in the average density of the droplet; the critical angle φ_* for bubble liquids, conversely, increases (Fig. 5).

3. Numerical Modeling of the Impact. The approaches employed in the previous sections enable one to investigate just the initial stage of impact of a droplet, providing the possibility of finding the values of the parameters sought at individual points of the flow. A more comprehensive idea of the impact can be obtained from a computational experiment by solving numerically the general system of partial equations [8] which describes the spreading of a bubble liquid over an obstacle. We note that in the literature [3–5] there are data on numerical modeling of the impact just for droplets of a liquid without gas occlusions. Furthermore, in the works mentioned no account has been taken of the action of the air around a droplet which, as is shown below, can have a significant influence on the process of interaction of the droplet with the obstacle.

Let a cylindrical droplet of water with the initial volume gas content α_0 strike against a rigid plane with its lower end at the instant of time $t = 0$. The velocity of impact of the droplet is 50 m/sec. We place the origin of the coordinate system at a point at the intersection of the collision plane and the axis of symmetry of the droplet. We guide the axis of symmetry Ox toward the motion of the droplet. The geometric dimensions of the droplet are as follows: height $h = 2$ mm and radius $R = 1$ mm. The droplet is surrounded by air under normal conditions. The calculations are carried out for droplets with an initial volume content of the gas of 0.2 and 0.3. For the problem in question with a relatively low impact velocity and a comparatively high gas content the compressibility of the carrier liquid can be disregarded. The corresponding system of equations describing the spreading of the droplet of a bubble liquid and the motion of a gas near it has the form

$$\frac{\partial \rho y}{\partial t} + \frac{\partial \rho u y}{\partial x} + \frac{\partial \rho v y}{\partial y} = 0 ,$$

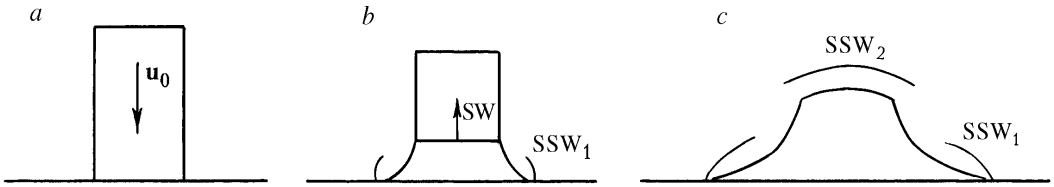

Fig. 6. Scheme of spreading of a cylindrical droplet over an obstacle.

$$\frac{\partial \rho u y}{\partial t} + \frac{\partial (p + \rho u^2) y}{\partial x} + \frac{\partial \rho u v y}{\partial y} = 0 ,$$

$$\frac{\partial \rho v y}{\partial t} + \frac{\partial \rho u v y}{\partial x} + \frac{\partial (p + \rho v^2) y}{\partial y} = p , \qquad (15)$$

$$\frac{\partial \rho e y}{\partial t} + \frac{\partial (\rho e + p) u y}{\partial x} + \frac{\partial (\rho e + p) v y}{\partial y} = 0 ,$$

$$\frac{\partial (1 - \alpha) y}{\partial t} + \frac{\partial (1 - \alpha) u y}{\partial x} + \frac{\partial (1 - \alpha) v y}{\partial y} = 0 ,$$

where $e = \varepsilon + (u^2 + v^2)/2$ is the total specific energy of the mixture and u and v are the projections of the velocity vector of the mixture onto the coordinate axes a and y. The first four equations of system (15) represent the laws of conservation for the entire mixture, while the last equation is the continuity equation for the incompressible liquid fraction. System (15) is considered simultaneously with the equation of state

$$\varepsilon = \frac{\alpha p}{(\gamma - 1)\rho} + \frac{(1 - a)\rho_1^0 \varepsilon_1}{\rho} ,$$

where ρ_1^0 and ε_1 are the true density and the specific internal energy of the liquid component. The latter was assumed to be constant. The calculations were carried out on a grid of 40×40 cells by the modified method of S. K. Godunov [11] in which the problem of decay of an arbitrary discontinuity in a gas-liquid mixture is employed as the mass operation. For the binary mixture with an incompressible liquid fraction considered in the work the solution of the corresponding Riemann problem has been given in [12].

Figure 6 shows schematically the picture of collision of the initially cylindrical droplet which touched the obstacle surface with its lower end at the instant of time $t = 0$ (Fig. 6a).

On impact, a plane SW moving from the contact surface to the upper end of the droplet (Fig. 6b) with velocities of 153 m/sec at $\alpha_0 = 0.3$ and 253 m/sec at $\alpha_0 = 0.2$ (which coincide with those calculated from the formula (4) of one-dimensional theory) is formed. The pressure at the center of the droplet, which is equal to 72.2 and 122.2 atm respectively, also coincides with the pressures calculated from the one-dimensional relation (2). The parameter distributions along the axis of symmetry and on the obstacle which have been obtained in the calculations by the instant of time $t = 4$ μsec for droplets with different gas contents are given in Fig. 7. The SW is followed by an unloading wave coming on the source side of the lateral surface of the droplet; this unloading wave gradually decreases the pressure behind the SW front, turning the liquid in the direction parallel to the collision plane, which is seen in Fig. 8a (cells occupied by the bubble liquid differ visually from those which contain a "pure" gas). Reaching the upper end of the droplet by the SW is accompanied by the retardation of liquid particles near the upper end and by the subsequent change of the direction of their motion near the axis of symmetry to the opposite, i.e., from the obstacle, which leads to the formation of a secondary SW (SSW_2) propagating in the gas in the direction from the obstacle (Fig. 6c). In Fig. 8b, one can see the secondary SW propagating in air from the droplet, which is also observed in the experiments [13, 14]. It is obvious that the amplitude of the secondary SW depends on the longitudinal dimension of the droplet: the larger the dimension, the more attenuated (by the rarefaction wave) the SW comes to the upper end of the droplet; consequently, the amplitude of the secondary SW will also be lower. The appearance of another secondary SW

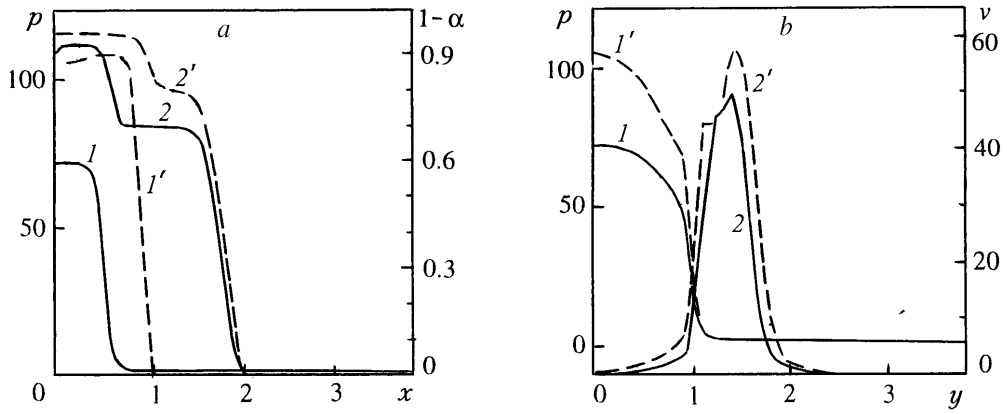

Fig. 7. Dependences of p and of the volume fraction of the liquid fraction on x (1 and 2 respectively) (a) and the dependences of p and v on y (1 and 2) (b) by an instant of time of 4 μsec at $\alpha_0 = 0.3$; curves $1'$ and $2'$, for the droplet with $\alpha_0 = 0.2$. p, atm; x, y, mm.

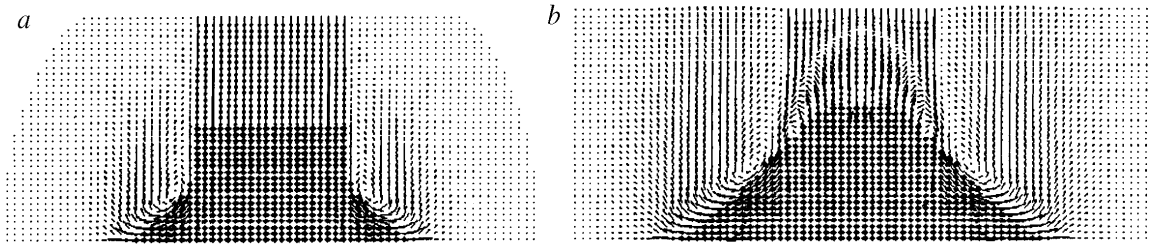

Fig. 8. Velocity fields at characteristic instants of time of 9.1 (a) and 19.1 μsec (b) on impact of a droplet ($\alpha_0 = 0.2$) against a rigid obstacle.

(SSW_1) recorded in the experiments for a spherical droplet [13] is less pronounced in the calculations for a cylindrical droplet. The reason is that in the case of impact of a cylindrical droplet the velocity of spreading of the liquid over the obstacle is substantially lower than that for a spherical droplet. Namely: the high-velocity jet of the liquid spreading over the obstacle is responsible for the formation of the secondary SW.

Figure 9 gives the time dependences of the pressure, the fraction of the liquid in the droplet near the obstacle on the axis of symmetry, and the impulse of force (momentum) acting on the surface of the solid body. The latter is calculated from the formula

$$I(t) = \int_0^t \iint_{S_c} p\,ds\,dt,$$

where S_c is the area of the spot of contact of the droplet with the obstacle surface.

We consider the variant of calculation with a shifted droplet; the interaction picture will be more complex as compared to the case described above. Let the droplet, at the instant of time $t = 0$, be at a distance of 1.5 m above the obstacle surface. The motion of the droplet to the obstacle is accompanied by the escape of the gas from the gap between the lower end of the droplet and the obstacle. The highest pressure in the gap is attained in the vicinity of the axis of symmetry, because of which the maximum deformation of the free surface of the droplet is observed precisely near the droplet axis. That is why the droplet entrains an air bubble at the instant of its collision with the obstacle. The presence of the air bubble changes the quantitative characteristics of a spreading droplet, which is clear from Fig. 9. In particular, the values of the pressure at the center of the impact turn out to be lower and the momentum acting on the obstacle on the source side of the droplet also decreases.

According to the results of the works, we can draw the following conclusions. The influence of the content of gas in the mixture on the parameters of a hydraulic shock for droplets with both a plane base and a convex base

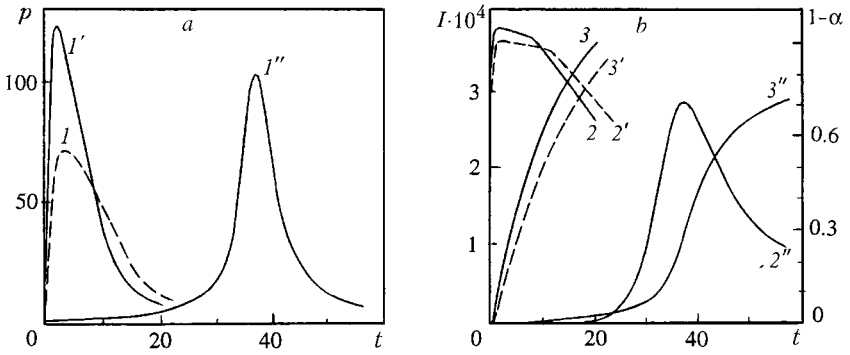

Fig. 9. Dependences of p on t (a) and the dependences of the volume fraction of the liquid at the origin of coordinates (2) and of I on t (3) at $\alpha = 0.3$; curves 1–3′, for a droplet with $\alpha = 0.2$; curves 1″–3″ for a shifted droplet at $\alpha_0 = 0.2$. p, atm; t, μsec.

has been studied. It has been shown that the presence of even a low amount of gas in the mixture eliminates the possibility of employing an acoustic approximation widely used for liquids without gas occlusions. It has been noted that in a number of cases one must take into account the air around the droplet, which can substantially change the picture of interaction of the droplet with the obstacle.

This work was carried out with financial support from the Russian Foundation for Basic Research (project code 00-01-00523).

NOTATION

p, pressure, Pa; u, velocity, m/sec; r, bubble radius, m; t, time, sec; ρ, density of the mixture, kg/m^3; α, volume fraction of the gas in the mixture; ρ_i^0, true density of the individual component, kg/m^3; φ, angle of inclination of the free droplet surface to the obstacle, deg; ψ, angle of inclination of the velocity vector to the Oy axis, deg; β_1 and β_2, angles of inclination of the attached shock waves, deg; δ, angle characterizing the deformation of the obstacle, deg; S, area, m^2; I, momentum, N·sec. Subscripts and superscripts: 0, initial state; 1, liquid component of the mixture; 2, obstacle; •, constant of the equation of state; *, critical value; n and t, normal and tangential components of the velocity vector; c, contact boundary.

REFERENCES

1. R. I. Nigmatulin, A. A. Gubaidulin, A. T. Akmetov, et al., *Dokl. Ross. Akad. Nauk*, **346**, No. 1, 46–50 (1996).
2. R. I. Nigmatulin, *Dynamics of Multiphase Media* [in Russian], Pt. 2, Moscow (1987).
3. A. L. Gonor and V. Ya. Rivkind, in: *Advances in Science and Technology, Ser. Mechanics of Liquids and Gases* [in Russian], Vol. 17, VINITI, Moscow (1982), pp. 86–159.
4. V. S. Surov and S. G. Ageev, *Izv. Sib. Otd. Akad. Nauk SSSR, Ser. Tekh. Nauk*, Issue 4, 66–71 (1989).
5. A. V. Chizhov and A. A. Shmidt, *Zh. Tekh. Fiz.*, **70**, Issue 12, 18–27 (2000).
6. M. B. Lesser, *Proc. Roy. Soc. London A*, **377**, 289–308 (1981).
7. A. A. Korobkin, *Phil. Trans. Roy. Soc. London A*, **355**, 507–522 (1997).
8. V. S. Surov, *Zh. Tekh. Fiz.*, **68**, Issue 11, 12–19 (1998).
9. F. H. Heymann, *J. Appl. Phys.*, **40**, No. 13, 5113–5121 (1969).
10. V. S. Surov and S. G. Ageev, *Izv. Vyssh. Uchebn. Zaved., Energetika*, No. 2, 103–106 (1989).
11. V. S. Surov, *Teplofiz. Vys. Temp.*, **36**, No. 2, 272–278 (1998).
12. V. S. Surov, *Fiz. Goreniya Vzryva*, **33**, No. 1, 143–147 (1997).
13. I. A. Dukhovskii, P. I. Kovalev, and A. A. Shmidt, *Pis'ma Zh. Tekh. Fiz.*, **10**, Issue 11, 649–652 (1984).
14. I. A. Dukhovskii and P. I. Kovalev, *Dokl. Akad. Nauk SSSR*, **297**, No. 3, 559–562 (1987).